Nonlinear dynamical analysis of a fluid-structure computational model with sloshing and capillarity

Quentin Akkaoui, Evangéline Capiez-Lernout, Christian Soize, Roger Ohayon

Nonlinear dynamical analysis of a fluid-structure computational model with sloshing and capillarity

Q. Akkaoui[1], **E. Capiez-Lernout**[1], **C. Soize**[1], **R. Ohayon**[2]
[1] Laboratoire Modélisation et Simulation Multi Echelle (MSME) UMR 8208 CNRS, 5 Boulevard Descartes 77454 Marne-La-Vallée, France
e-mail: **quentin.akkaoui@univ-paris-est.fr**

[2] Structural Mechanics and Coupled System Laboratory, Conservatoire National des Arts et Métiers (CNAM), 2 rue Conté, 75003, Paris , France

Abstract
This paper deals with a computational methodology for analyzing a fluid-structure system taking into account sloshing and capillarity phenomena. The fluid is assumed to be linear acoustic and the structure is assumed to undergo large displacements/deformations, which induce geometrical nonlinearities in the fluid-structure system. An adapted nonlinear reduced-order model is constructed using a modal characterization of each part of the coupled system. A numerical application is considered in order to study the effects of the geometrical nonlinearities on the dynamical forced response of the structural acoustic system.

1 Introduction

The understanding of fluid-structure dynamic interactions has always received a great attention and is of fundamental interest with respect to numerous applications (see for instance [2, 14, 10]). In particular, the sloshing phenomenon and the influence of the surface tension on the vibrational motion of the free surface of a fluid have been widely studied these last decades (see [10, **?**, 6, 12]). Note that the physics and modeling of surface tension can be found, for instance, in [7, 8]. The present work is devoted to a computational nonlinear dynamical analysis of a fluid-structure system, for which the fluid is a liquid is presence of a gravity field, taking into account both surface tension and sloshing effects. The structure is assumed to undergo large displacements and large deformations that could possibly influence the dynamical response of the fluid-structure system. Hence, the formulation used to analyze such fluid-structure system is the one recently proposed in [12, 13] that allows for considering the geometrical nonlinearities related to the structure through the use of an adapted computational nonlinear reduced-order model. This nonlinear reduced-order model relies on projecting the fluid-structure boundary value problem onto an adapted reduced-order basis that is constructed by considering several generalized eigenvalue problems related to the dynamics of the structure, of the acoustic fluid, and of the free surface. A detailed computational methodology for constructing this projection basis in the context of large scale fluid-structure systems has been proposed and validated in [1].

The computational model is constructed with the finite element method [15, 9] for which the unknowns of the problem are the nonlinear displacements of the elastic structure, the acoustic pressure in the liquid, and the free-surface normal elevation of the liquid. Furthermore, each reduced operator (linear or nonlinear) of the reduced-order computational model is explicitly calculated. The algorithm for solving the nonlinear reduced-order computational model uses simultaneously the arc-length algorithm (see [5]) and the fixed-point method.

The paper is organized as follows. Section 2 is dedicated to the formulation of the fluid-structure problem. In

particular, the construction of the nonlinear reduced-order model is explained in details. Section 3 is devoted to a numerical application that consists in a large scale computational model of an elastic cylindrical tank partially filled with the liquid (water). The nonlinear response of the fluid-structure system is analyzed in details.

2 Formulation of the fluid-structure problem

2.1 Notations and hypotheses

The equations of the fluid-structure system are written with a total Lagrange formulation and the related *reference configuration* is described in Figure 1. The structure, which is taken in its natural state without prestresses, occupies a bounded domain Ω_S and is assumed to be constituted of a homogeneous isotropic linear viscoelastic material without memory. The structure contains a linear dissipative acoustic fluid occupying a bounded domain Ω_F. Gravitational and surface tension effects are taken into account in the present formulation but internal gravity waves are neglected. It should be noted that the geometry of the free surface is obtained by a pre-computation allowing the static equilibrium to be found. The acoustic fluid is assumed to be dissipative. This dissipation is modeled by an equivalent damping term in the Helmholtz equation [11].

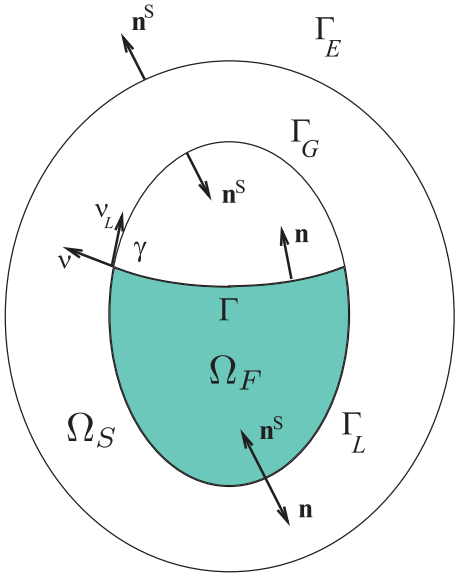

Figure 1: Reference configuration of the fluid-structure system (figure from [13])

The boundary of Ω_F is written as $\partial\Omega_F = \Gamma_L \cup \gamma \cup \Gamma$ (with $\Gamma_L \cap \gamma = \varnothing$, $\Gamma \cap \gamma = \varnothing$, $\Gamma_L \cap \Gamma = \varnothing$), where Γ_L is the fluid-structure interface, Γ is the free surface of the fluid and γ is the contact line between the structure and the fluid. The boundary of Ω_S is denoted by $\partial\Omega_S = \Gamma_E \cup \Gamma_L \cup \gamma \cup \Gamma_G$, where Γ_E and Γ_G are the external structural boundary of the structure and the part of the internal structural boundary that is not in contact with the fluid. The structure is submitted to a given body force field $\mathbf{b}$ in Ω_S and to a given surface force field $\mathbf{f}$ on Γ_E. The external unitary normals to $\partial\Omega_S$ and $\partial\Omega_F$ are denoted by $\mathbf{n}^S$ and $\mathbf{n}$. Let $\boldsymbol{\nu}$ and $\boldsymbol{\nu}_L$ be the external unit normals to γ belonging respectively to the tangent plane to Γ and to the tangent plane to Γ_L. The structure is assumed to be fixed on a part of its boundary Γ_E. We are then interested in analyzing the vibrations of the coupled fluid-structure system around its reference configuration.

Let $\mathbf{x} = (x_1, x_2, x_3)$ be the generic point in a Cartesian reference system $(\mathbf{O}, \mathbf{e}_1, \mathbf{e}_2, \mathbf{e}_3)$. The gravity vector is $\mathbf{g} = -g\,\mathbf{e}_3$ with $g = \| \mathbf{g} \|$. The boundary value problem is expressed in terms of the structural displacement

field $\mathbf{u}(\mathbf{x},t)$, of the internal pressure field $p(\mathbf{x},t)$, and of the normal displacement field of the free surface $\eta(\mathbf{x},t)$. In order to simplify the notations, the convention for summation over repeated Greek and Latin indices is considered and parameters $\mathbf{x}$ and t are removed if there is no possible confusion. Let $a(\mathbf{x},t)$ be a given function, the following notations are used : $a_{,j} = \partial a/\partial x_j$, $\dot{a} = \partial a/\partial t$ and $\ddot{a} = \partial^2 a/\partial t^2$.

2.2 Finite element computational model

In this work, the computational model is constructed with the finite element method. We are interested in analyzing the nonlinear forced response of the fluid-structure system and the equations are formulated in the time domain. Let $n_{PHS} = n_P + n_H + n_S$ be the total number of dof on the computational model, where n_P, n_H, and n_S correspond to the number of dofs of the fluid, of the free surface, and of the structure. We then denote by $\mathbb{P}$, $\mathbb{H}$, and $\mathbb{U}$ the $\mathbb{R}^{n_P}$-vector, $\mathbb{R}^{n_H}$-vector, and the $\mathbb{R}^{n_S}$-vector corresponding to the finite element discretization of the pressure field in the acoustic fluid, of the normal elevation of the free surface, and of the nonlinear structural displacement. The computational finite element model of the fluid-structure system is then described by the following set of nonlinear coupled differential equations,

$$[M]\,\ddot{\mathbb{P}} + [D]\,\dot{\mathbb{P}} + [K]\,\mathbb{P} - [C_{p\eta}]^T\,\ddot{\mathbb{H}} - [C_{pu}]^T\,\ddot{\mathbb{U}} = 0\,, \tag{1}$$

$$[C_{p\eta}]\,\mathbb{P} + [K_{gc}]\,\mathbb{H} + [C_{\eta u}]\,\mathbb{U} = 0\,, \tag{2}$$

$$[C_{pu}]\,\mathbb{P} + [C_{\eta u}]^T\,\mathbb{H} + [M_S]\,\ddot{\mathbb{U}} + [D_S]\,\dot{\mathbb{U}} + [K_S]\,\mathbb{U} + \mathbb{F}_{NL}(\mathbb{U}) = \mathbb{F}_S\,. \tag{3}$$

In Eq. (1), the $(n_P \times n_P)$ symmetric positive definite matrix $[M]$ is the fluid mass matrix. The $(n_P \times n_P)$ symmetric positive semidefinite matrices $[D] = \tau[K]$ and $[K]$ are the damping and stiffness matrices of the fluid, in which τ is the acoustic damping coefficient. In Eq. (2), the $(n_H \times n_H)$ symmetric positive definite matrix $[K_{gc}]$ is the matrix related to the sloshing/capillarity effects on the free surface. In Eq. (3), the $(n_S \times n_S)$ symmetric positive definite matrices $[M_S]$, $[D_S] = \tau_S[K_S]$, and $[K_S]$ are the mass, damping, and stiffness matrices of the structure with τ_S the elastic damping coefficient. The rectangular $(n_S \times n_P)$, $(n_H \times n_P)$, and $(n_H \times n_S)$ real matrices $[C_{pu}]$, $[C_{p\eta}]$, and $[C_{\eta u}]$ are the coupling matrices between the fluid and the structure, between the fluid and the free surface, and between the structure and the free surface. In Eq. (3) the $\mathbb{R}^{n_S}$-vectors $\mathbb{F}_S$ and $\mathbb{F}_{NL}(\mathbb{U})$ correspond to the discretization of the external force field applied to the structure and to the nonlinear internal forces in the structure induced by the geometrical nonlinearities.

The numerical resolution of the set of nonlinear coupled differential equations (Eqs.(1) to (3)) appears to be time consuming or even impossible when considering large finite element models. It is thus essential to introduce an efficient reduced-order model.

2.3 Nonlinear reduced-order computational model

The nonlinear reduced-order model is constructed by projecting the equations on an adapted reduced-order basis, whose basis vectors are represented by the $(n_{PHS} \times N_{PHS})$ real matrix $[\Psi]$. The corresponding approximated solution is denoted by the $\mathbb{R}^{n_{PHS}}$-vector $(\mathbf{P},\mathbf{H},\mathbf{U})$ that is written as follows

$$\begin{bmatrix}\mathbf{P}\\ \mathbf{H}\\ \mathbf{U}\end{bmatrix} = \begin{bmatrix}[\Phi_P] & [\Phi_{PH}] & 0\\ 0 & [\Phi_H] & 0\\ 0 & 0 & [\Phi_S]\end{bmatrix}\begin{bmatrix}\mathbf{q}^P\\ \mathbf{q}^H\\ \mathbf{q}^U\end{bmatrix} = [\Psi]\,\mathbf{Q}\,, \tag{4}$$

in which the $\mathbb{R}^{N_P}$-vector $\mathbf{q}^P$, the $\mathbb{R}^{N_H}$-vector $\mathbf{q}^H$, and the $\mathbb{R}^{N_S}$-vector $\mathbf{q}^U$ are the generalized coordinates. The total number of generalized coordinates is $N_{PHS} = N_P + N_H + N_S$. In Eq. (4), the $(n_P \times N_P)$ real matrix $[\Phi_P]$ is made up of the acoustic modes of the internal fluid, the $(n_H \times N_H)$ real matrix $[\Phi_H]$, of the sloshing modes of the free surface, and the $(n_S \times N_S)$ real matrix $[\Phi_S]$, the eigenmodes of the linearized structure for which the added mass matrix effect is taken into account [10]). It should be noted that the $(n_P \times N_H)$ real matrix $[\Phi_{PH}]$ is made up of the corresponding acoustic part associated with each sloshing modes. For

more details concerning the computational aspects of the construction of such proposed reduced-order basis, we refer the reader to [1]. The $\mathbb{R}^{N_{PHS}}$-vector $\mathbf{Q} = (\mathbf{q}^P, \mathbf{q}^H, \mathbf{q}^U)$ is then solution of the following set of N_{PHS} nonlinear coupled differential equations

$$[\mathscr{M}_{FSI}]\,\ddot{\mathbf{Q}}(t) + [\mathscr{D}_{FSI}]\,\dot{\mathbf{Q}}(t) + [\mathscr{K}_{FSI}]\,\mathbf{Q}(t) + \mathscr{F}_{NL}(\mathbf{Q}(t)) = \mathscr{F}(t)\,, \tag{5}$$

in which the $(N_{PHS} \times N_{PHS})$ matrices $[\mathscr{M}_{FSI}]$, $[\mathscr{D}_{FSI}]$, $[\mathscr{K}_{FSI}]$, and the $\mathbb{R}^{N_{PHS}}$ vectors $\mathscr{F}$ and $\mathscr{F}_{NL}$ are such that

$$[\mathscr{M}_{FSI}] = [\Psi]^T \begin{bmatrix} [M] & -[C_{p\eta}]^T & -[C_{pu}]^T \\ 0 & 0 & 0 \\ 0 & 0 & [M_S] \end{bmatrix} [\Psi]\,, \tag{6}$$

$$[\mathscr{D}_{FSI}] = [\Psi]^T \begin{bmatrix} [D] & 0 & 0 \\ 0 & 0 & 0 \\ 0 & 0 & [D_S] \end{bmatrix} [\Psi]\,, \tag{7}$$

$$[\mathscr{K}_{FSI}] = [\Psi]^T \begin{bmatrix} [K] & 0 & 0 \\ [C_{p\eta}] & [K_{gc}] & [C_{\eta u}] \\ [C_{pu}] & [C_{\eta u}]^T & [K_S] \end{bmatrix} [\Psi]\,, \tag{8}$$

$$\mathscr{F}(t) = [\Psi]^T \begin{bmatrix} 0 \\ 0 \\ \mathbb{F}_S(t) \end{bmatrix}\,, \tag{9}$$

$$\mathscr{F}_{NL}(\mathbf{Q}(t)) = [\Psi]^T \begin{bmatrix} 0 \\ 0 \\ \mathbb{F}_{NL}(\mathbf{Q}(t)) \end{bmatrix}\,. \tag{10}$$

In Eq. (5), vector $\mathscr{F}_{NL}(\mathbf{Q}(t))$ denotes the nonlinear internal forces induced by the geometrical nonlinearities of the structural part that are computationally constructed from the knowledge of the nonlinear reduced operators [4].

3 Numerical Application

3.1 Computational finite element model

The fluid-structure system is constituted of a thin circular cylindrical tank made up of aluminum. This cylinder is closed at both ends by a circular aluminum disk. Let $R_i = 0.03\,m$ and $e_{cyl} = 10^{-4}\,m$ be the internal radius of the cylinder and its thickness. Let $e_b = 2 \times 10^{-4}\,m$ be the thickness of the two circular aluminum disk at the top and at the bottom. The total height of the cylinder is $h = 0.1504\,m$. The Young modulus of aluminum is $E = 62 \times 10^9\,N.m^{-2}$, Poisson ratio $\nu = 0.33$, mass density $\rho_S = 2{,}700\,Kg.m^{-3}$, and damping coefficient $\tau_S = 10^{-6}\,s$. This tank is partially filled (at 30%) with water (see Figure 2)for which the sound velocity is $c_0 = 1{,}480\,m.s^{-1}$, mass density $\rho_0 = 1{,}000\,Kg.m^{-3}$, damping coefficient $\tau = 10^{-6}\,s$, surface tension coefficient $\sigma_\Gamma = 7.28 \times 10^{-2}\,N.m^{-1}$, and the contact angle between water and aluminum is $\alpha = 70^\circ$. The origin O of the Cartesian coordinates system $(O, \mathbf{e}_1, \mathbf{e}_2, \mathbf{e}_3)$ is located at the center of the bottom of the cylindrical tank. Axis $\mathbf{e}_3$ coincides with the revolution axis of the tank. The equilibrium position of the fluid in the cylindrical tank is precomputed using the software Surface Evolver [3]. The cylinder is clamped at its bottom. The finite element model of the fluid-structure requires to use high orders elements due to the slenderness of the cylinder wall and of the high flexibility of the free surface motion. The finite element discretization of the system is thus constructed using 27-nodes 3D-solid finite elements for the structure and for the acoustic fluid. The free surface of the liquid is meshed using 9-nodes 2D finite elements and the triple line is meshed using 3-nodes 1D finite elements. Table 1 summarizes the numerical data concerning the finite element mesh.

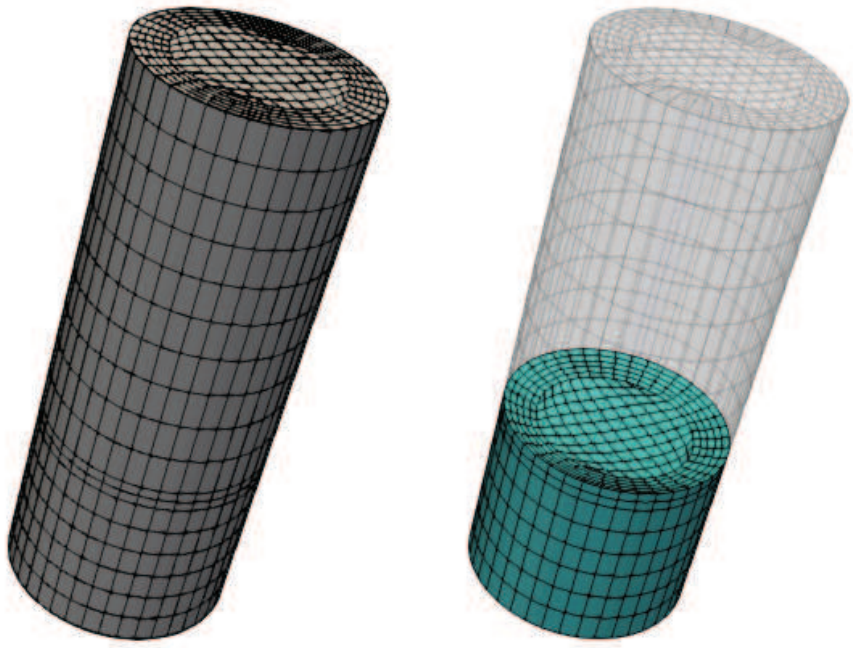

Figure 2: Finite element meshes of the structure (left) and of the liquid with its free surface (right).

	Nodes	**Dof**	**Elements**
Fluid	21,097	21,097	2,400
Free surface	1,241	1,241	300
Structure	16,806	50,418	1,400

Table 1: Table of the finite element mesh numerical data

3.1.1 Observation points

The dynamical response of the fluid-structure system is analyzed at different observation nodes. The first observation node is common to both structure and free surface, in order to see the coupling between the structural displacement and the elevation of the free surface. It is denoted by $\mathbf{x}_{H_1}^{obs}$ on the free surface and by $\mathbf{x}_{U}^{obs}$ on the structure. Then, two observation points denoted by $\mathbf{x}_{P_1}^{obs}$ and $\mathbf{x}_{P_2}^{obs}$, and corresponding to a node located at the fluid bottom and to a node located at mid-depth in the fluid are chosen. Finally, another observation node, denoted by $\mathbf{x}_{H_2}^{obs}$ and that is located at the center of the free surface is chosen. The coordinates of these observation points are summarized in Table 2. In the following, for the sake of clarity, the notations $\mathbf{P}_i$ and $\mathbf{H}_i$ are introduced for representing the pressure and the elevation of the free surface at the observation point $\mathbf{x}_{P_i}^{obs}$ and $\mathbf{x}_{H_i}^{obs}$ for $i = 1, 2$. The notation $\mathbf{U}_j$ is used for representing the component number j of the structural displacement observed at observation node $\mathbf{x}_{U}^{obs}$.

3.2 Computational reduced-order bases

The computational reduced-order basis $[\Psi]$ is constructed according to Section 2.3, by solving three generalized eigenvalue problems associated with $\mathbf{P}$, $\mathbf{H}$, and $\mathbf{U}$ [12, 1]. Some acoustic, sloshing, and elastic eigenmodes are represented with their respective eigenfrequencies denoted by ν_i^a, for $i = 1, \ldots, N_a$ with

Location	Name	x coordinate	y coordinate	z coordinate
Fluid	$\mathbf{x}_{P_1}^{obs}$	0.0147	0	0.0002
	$\mathbf{x}_{P_2}^{obs}$	0.0147	0	0.0185
Free surface	$\mathbf{x}_{H_1}^{obs}$	0	0.03	0.0497
	$\mathbf{x}_{H_2}^{obs}$	0	0	0.0452
Structure	$\mathbf{x}_{U}^{obs}$	0.0168	−0.0168	0.0467

Table 2: Localization of the observation nodes for the fluid, the structure and the free surface

$a \in \{P, H, S\}$.

3.2.1 Acoustic eigenmodes of the internal fluid

Figure 3 displays some acoustic eigenmodes of the liquid computed with zero pressure on the free surface, and their respective eigenfrequencies. For the present numerical application, it should be noted that the resonance of the internal fluid is a high-frequency phenomenon since the fundamental frequency of the fluid is $\nu_1^P = 7{,}824\,Hz$.

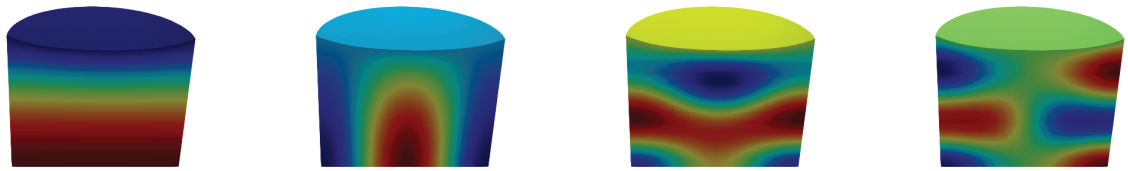

$\nu_1^P = 7{,}824\,Hz$ $\nu_9^P = 30{,}718\,Hz$ $\nu_{15}^P = 39{,}279\,Hz$ $\nu_{18}^P = 41{,}226\,Hz$

Figure 3: Example of acoustic modes of the internal fluid

3.2.2 Sloshing eigenmodes of the free surface

Figure 4 displays some sloshing modes of the free surface for which the fundamental eigenfrequency is $\nu_1^H = 3.68\,Hz$, which is of order 10^3 smaller than the fundamental frequency of the internal fluid. Moreover, it can be seen that the modal density of the sloshing is high since the 500-th eigenfrequency is $\nu_{500}^H = 56.38\,Hz$. The corresponding acoustic part of the sloshing modes $[\Phi_{PH}]$ is displayed in Figure 5. It can be seen that there is effectively an exponential decreasing of the pressure as function of the distance to the free surface.

3.2.3 Elastic eigenmodes of the structure

Figure 6 and 7 display some elastic eigenmodes of the structure related to the empty and the partially filled fluid-structure system. In particular, since these modes have been calculated by including the added mass effect induced by the fluid, this influence can be quantified regarding both modal shapes and relative eigenfrequencies. Note that the eigenmodes and the associated eigenfrequencies, whose modal contribution is concentrated at the top of the structure remain unchanged.

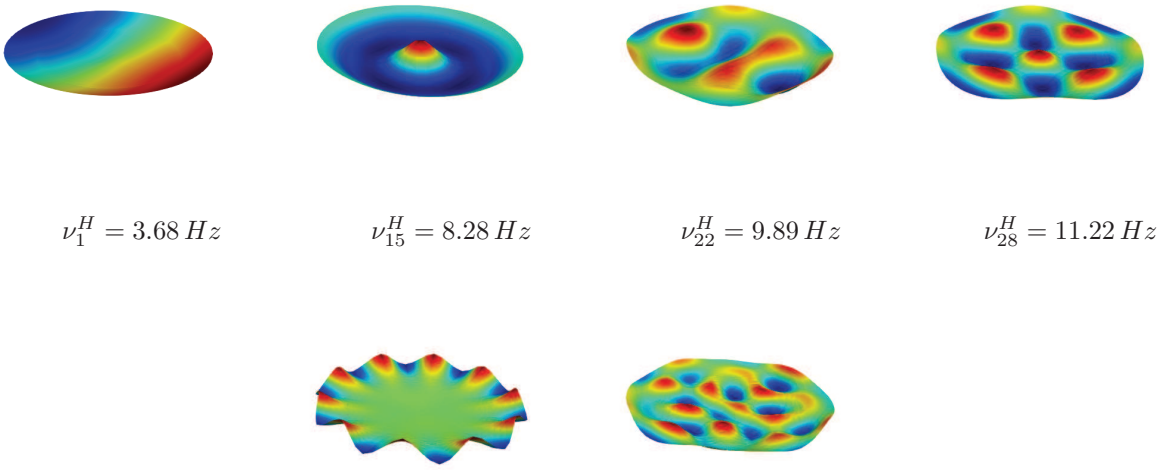

$\nu_1^H = 3.68\,Hz$ $\nu_{15}^H = 8.28\,Hz$ $\nu_{22}^H = 9.89\,Hz$ $\nu_{28}^H = 11.22\,Hz$

$\nu_{37}^H = 13.06\,Hz$ $\nu_{59}^H = 16.99\,Hz$

Figure 4: Example of sloshing modes of the free surface.

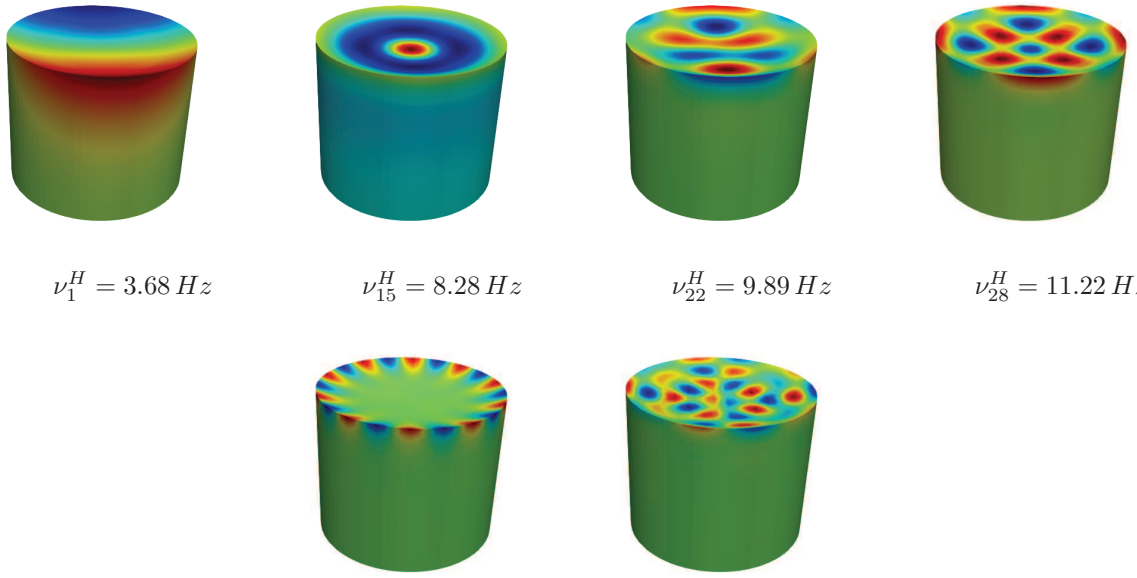

$\nu_1^H = 3.68\,Hz$ $\nu_{15}^H = 8.28\,Hz$ $\nu_{22}^H = 9.89\,Hz$ $\nu_{28}^H = 11.22\,Hz$

$\nu_{37}^H = 13.06\,Hz$ $\nu_{59}^H = 16.99\,Hz$

Figure 5: Example of corresponding acoustic part of the sloshing modes.

3.3 Dynamical excitation of the system

The dynamical excitation of the system is defined in the time domain and is chosen in order to uniformly excite a frequency band of interest that corresponds to some of the structural and sloshing resonances of the fluid-structure system. Since the fundamental sloshing eigenfrequency of the free surface is $\nu_1^H = 3.68\,Hz$ and since the fundamental frequency of the internal liquid is $\nu_1^P = 7{,}824\,Hz$, the time domain excitation is chosen such that the corresponding excitation frequency band is $\mathbb{B}_e = [\nu_{min}\,,\,\nu_{max}]\,Hz$, with $\nu_{min} = 15\,Hz$

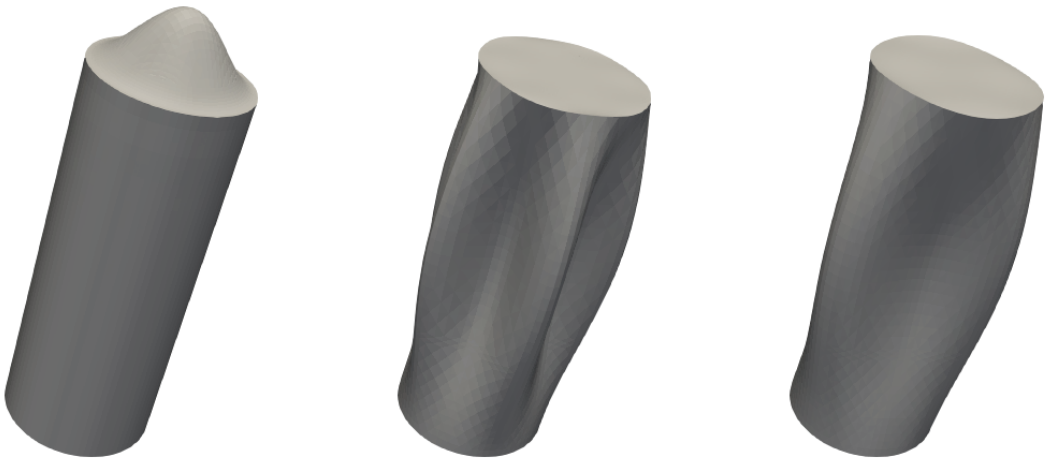

$\nu_1^S = 510\,Hz$ $\nu_7^S = 1{,}461\,Hz$ $\nu_9^S = 1{,}514\,Hz$

Figure 6: Example of elastic modes of the empty structure.

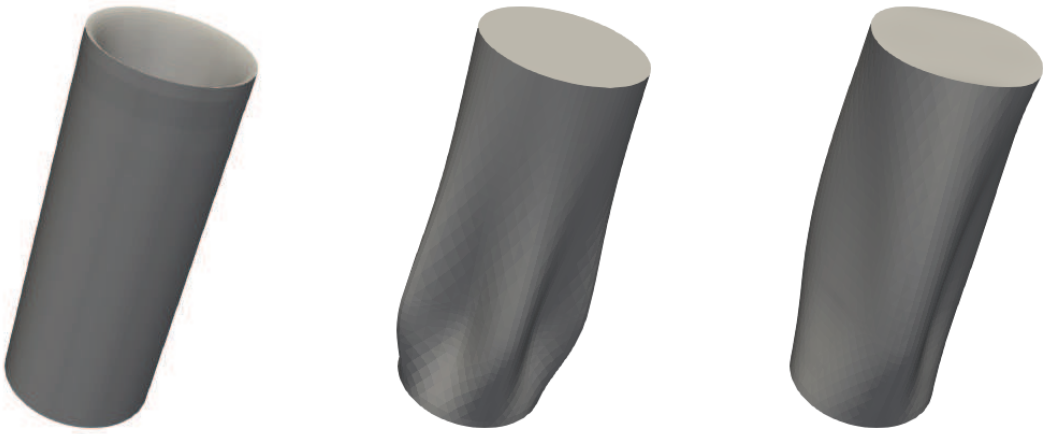

$\nu_8^S = 510\,Hz$ $\nu_5^S = 530\,Hz$ $\nu_9^S = 639\,Hz$

Figure 7: Example of elastic modes of the structure when considering the influence of the liquid.

and $\nu_{max} = 1{,}550\,Hz$. In this frequency band, the first 9 eigenmodes of the structure are excited. The dynamical excitation is located on the surface zone defined by $r = R + e_{cyl}$, $\theta \in [-\pi/32, \pi/32]$ and $x_3 = [h/2 - h_f, h/2 + h_f]$ with $h_f = 0.02\,m$ in cylindrical coordinates. Figure 8 displays the graph $t \mapsto g(t)$ of the time repartition of the excitation (whose maximum over the time domain is set to 1) and of its corresponding Fourier transform. It can be seen that such a choice allows the frequencies between $15\,Hz$ and $1{,}550\,Hz$ to be excited. The maximum load intensity is given by $f_0 = 2{,}000\,N$ that corresponds to subsequent nonlinear geometrical effects. The computations is carried out with a sampling frequency $\nu_e = 15{,}500\,Hz$ and with $n_t = 10^6$ time steps. The initial time is chosen as $t_{ini} = -1.30\,s$ yielding a null initial load and the time duration is chosen as $T = 67\,s$. Consequently, these computational parameters are adapted for observing the resonances related to the sloshing motion, which is also known to be a low-frequency and weakly damped phenomenon in the present numerical application. It should be noted that the nonlinear dynamical response of the fluid-structure system is calculated in the time domain with a Newmark algorithm for which the

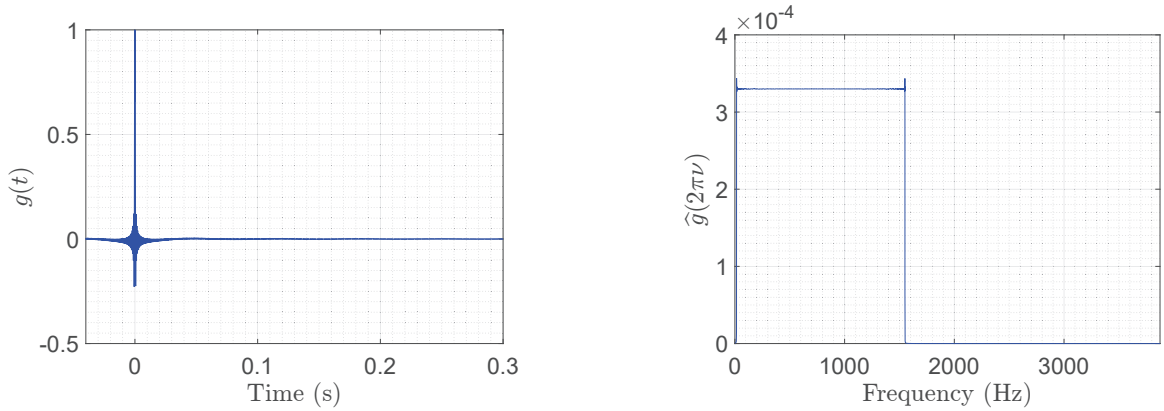

Figure 8: Graph of the dynamical excitation of the fluid-structure system (left) and its Fourier transform (right).

nonlinearity is solved using either the fixed point method or arc-length based algorithms. The nonlinear dynamical analysis is carried out *a posteriori* in the frequency domain by evaluating its Fourier transform from a FFT algorithm. The frequency band of analysis is given by $\mathbb{B}_a = [0\,,\,\nu_{max}]$ with $\nu_{max} = 5{,}000\,Hz$. In the following, the notation $\widehat{A}(2\pi\nu)$ denotes the Fourier transform of quantity $A(t)$.

3.4 Reduced-order model convergence

In order to construct an efficient reduced-order model, a convergence analysis is performed in order to determine the optimal number N_P, N_H, and N_S of bases vectors. Due to the large dimension of the finite element model, the computation of the solution $(\mathbb{P}, \mathbb{H}, \mathbb{U})$ of Eqs. (1) to (3) is not calculated. Thus, the solutions $(\mathbf{P}, \mathbf{H}, \mathbf{U})$ obtained by using the nonlinear reduced-order model cannot be compared to the reference solution. For circumventing this problem, we assume that the solution is converged for a high number of eigenmodes $N_P^{max} = 500$, $N_H^{max} = 500$, and $N_S^{max} = 200$. Then, three convergence analyses are performed with respect to N_P, N_H and N_S. In the following, the results presented are calculated using the optimal number of eigenmodes.

3.5 Linear and nonlinear dynamical responses of the fluid-structure system

The influence of the geometrical nonlinearities of the structure on the fluid-structure system is quantified by comparing the linear and the nonlinear dynamical responses of the fluid-structure system. The linear dynamical response of the system is calculated by solving the set of differential equations defined by Eq. (5) for which $\mathscr{F}_{NL}(\mathbf{Q}(t)) = 0$. These results are then compared to the nonlinear dynamical analysis of the fluid-structure system. For convenience, we denote by superscript L the quantities calculated for the linear system and by superscript *NL* the quantities calculated for the nonlinear system. Figure 9 displays the graphs of $\nu \mapsto |\widehat{P}_i^L(2\pi\nu)|$ (left figure) and of $\nu \mapsto |\widehat{P}_i^{NL}(2\pi\nu)|$ (right figure) for $i \in \{1, 2\}$. Figure 10 displays the graphs of $\nu \mapsto |\widehat{H}_i^L(2\pi\nu)|$ (left figure) and of $\nu \mapsto |\widehat{H}_i^{NL}(2\pi\nu)|$ (right figure) for $i \in \{1, 2\}$. Figure 11 displays the graphs of $\nu \mapsto |\widehat{U}_i^L(2\pi\nu)|$ (left figure) and of $\nu \mapsto |\widehat{U}_i^{NL}(2\pi\nu)|$ (right figure) for $i \in \{1, 2, 3\}$.

These results show that the geometrical nonlinearities that are taken into account in the computational modelling have a significant impact on the responses of the fluid-structure system. When considering the linear responses of the fluid-structure system, we clearly see that the resonances that are located in the excitation band $\mathbb{B}_e$ well match with the elastic and sloshing eigenfrequencies. The nonlinear responses of the fluid-structure system are more interesting. Unexpected resonances that are localized below and beyond $\mathbb{B}_e$ appear. Moreover, their contribution appear to be significative with resonance amplitudes of the same order as the resonance amplitudes that are localized in $\mathbb{B}_e$.

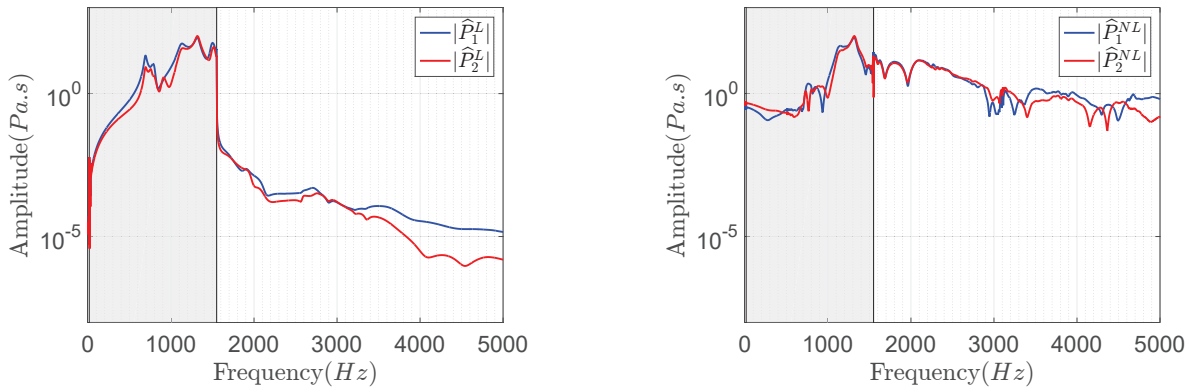

Figure 9: Graph of the linear (left) and nonlinear (right) FRF of the pressure in the internal liquid seen at the observation points.

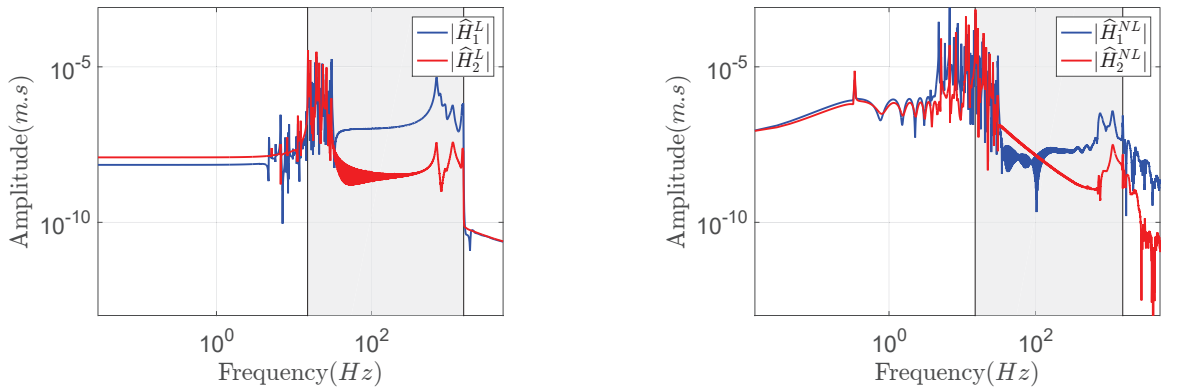

Figure 10: Graph of the linear (left) and nonlinear (right) FRF of the elevation of the free surface seen at the observation points.

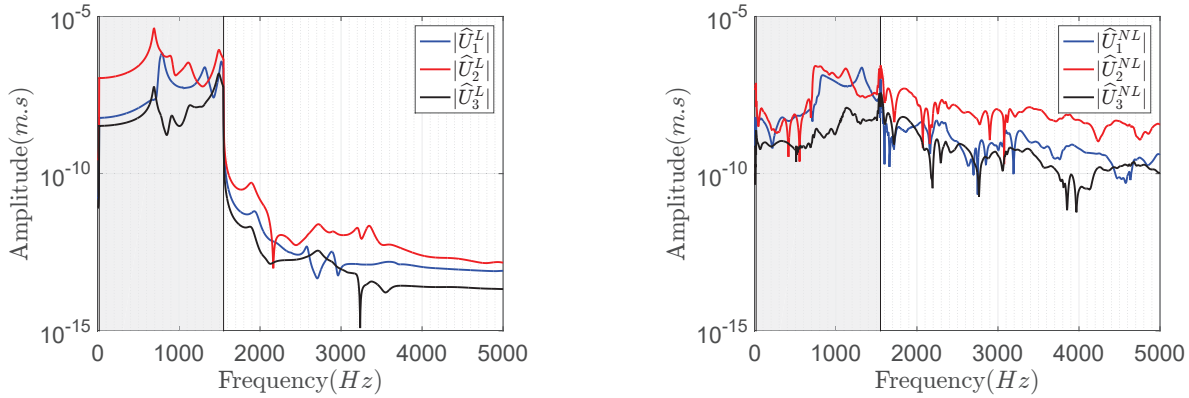

Figure 11: Graph of the linear (left) and nonlinear (right) FRF of the structural displacement seen at the observation point.

4 Conclusion

This paper proposes a computational methodology adapted to a fluid-structure system for which sloshing and capillarity effects are taken into account and for which the structure is assumed to undergo large displace-

ments/deformations. The construction of an adapted nonlinear reduced-order model is required for reducing the computational costs, mostly if large finite element models are considered. The formulation used for such nonlinear reduced-order model allows for constructing a projection basis for each part of the fluid-structure system in order to circumvent the possible gap between the eigenfrequencies of each sub-system. This means that if the eigenmodes of the coupled fluid-structure system were directly calculated, about ten thousands eigenmodes should be computed in the considered frequency band of analysis instead of the 500 that have been computed. In addition, the mesh should considerably be refined for computing this huge number of sloshing modes. The numerical application constituted of a cylindrical tank partially filled with a fluid demonstrate the efficiency of the proposed method. In particular, the results show that the responses are strongly modified by the presence of the geometrical nonlinearities.

Acknowledgements

This work has been supported by the DGA (French defence procurement agency) in the context of a PhD thesis.

References

[1] Q. Akkaoui, E. Capiez-Lernout, C. Soize, and R. Ohayon. Solving generalized eigenvalue problems for large scale fluid-structure computational models with mid-power computers. *Computers & Structures*, 205:45–54, 2018.

[2] H. Berger, R. Ohayon, and J. Boujot. On a spectral problem in vibration mechanics-computation of elastic tanks partially filled with liquids. *Journal of Mathematical analysis and applications*, 51:272–298, 1975.

[3] K. A. Brakke. The surface evolver. *Experimental mathematics*, 1(2):141–165, 1992.

[4] E. Capiez-Lernout, C. Soize, and M. Mignolet. Computational stochastic statics of an uncertain curved structure with geometrical nonlinearity in three-dimensional elasticity. *Computational Mechanics*, 49(1):87–97, 2012.

[5] M. A. Crisfield, J. J. Remmers, C. V. Verhoosel, et al. *Nonlinear finite element analysis of solids and structures*. John Wiley & Sons, 2012.

[6] C. Farhat, E. K.-Y. Chiu, D. Amsallem, J.-S. Schotté, and R. Ohayon. Modeling of fuel sloshing and its physical effects on flutter. *AIAA journal*, 51(9):2252–2265, 2013.

[7] R. Finn. The contact angle in capillarity. *Physics of Fluids*, 18(4):047102, 2006.

[8] R. Finn and G. K. Luli. On the capillary problem for compressible fluids. *Journal of Mathematical Fluid Mechanics*, 9(1):87–103, 2007.

[9] T. J. Hughes. *The finite element method: linear static and dynamic finite element analysis*. Courier Corporation, 2012.

[10] H. J. Morand and R. Ohayon. *Fluid Structure Interaction*. John Wiley & Sons, New York, 1995.

[11] R. Ohayon and C. Soize. Structural acoustic and vibration, 1998.

[12] R. Ohayon and C. Soize. Vibration of structures containing compressible liquids with surface tension and sloshing effects. Reduced-order model. *Computational Mechanics*, 55(6):1071–1078, 2015.

[13] R. Ohayon and C. Soize. Nonlinear model reduction for computational vibration analysis of structures with weak geometrical nonlinearity coupled with linear acoustic liquids in the presence of linear sloshing and capillarity. *Computers & Fluids*, 141:82 – 89, 2016.

[14] L. G. Olson and K. J. Bathe. Analysis of fluid-structure interactions - a direct symmetric coupled formulation based on a fluid velocity potential. *Computers & Structures*, 21:21–32, 1985.

[15] P. Wriggers. *Nonlinear finite element methods*. Springer Science & Business Media, 2008.